# Isolated Rotor Forward Flight Testing From One Atmosphere Down to Martian Atmospheric Densities

Geoffrey A. Ament Witold J. F. Koning
*Science and Technology Corporation*
NASA Ames Research Center
Moffett Field, California

**Abstract**

**With the recent interest in Martian exploration using unmanned aerial vehicles, an experimental study was conducted to investigate rotor performance at Martian atmospheric conditions. Both simulation and testing of rotors is vital for the evaluation of performance and behavior of a rotor, especially for operations at Martian atmospheric density and pressure. One critical test that has not been performed to date is helicopter forward flight testing at Martian atmospheric densities. To achieve this, a test was conducted in a tunnel facility which could be evacuated to the atmospheric pressure and density of Mars. A 40-in diameter rotor, roughly approximating the proposed Mars Helicopter design by the NASA Jet Propulsion Laboratory, was tested in forward flight at Mars atmospheric pressure at the NASA Ames Planetary Aeolian Laboratory. The goal of this experiment was to collect rotor thrust, rotational speed, power, torque, and acoustics measurements. Subsequently, these results are correlated with simulated cases using a mid-fidelity computational fluid dynamics simulation. As expected, rotor thrust and power are drastically reduced at air densities 100 times lower than at sea level on Earth. In addition, Reynolds number effects seem to play a vital role at reduced pressure that cannot be neglected in the simulation.**

## Introduction

In the interest of exploring and learning more about our solar system, NASA has executed several unmanned missions to Mars. Among these successes, various missions to Mars have allowed for close examination of the Martian surface, and one rover is still in operation today. Unfortunately, due to Mars' rocky terrain and communication delays between Earth and Mars, it can prove difficult to efficiently move around on the Martian surface. In an effort to help resolve these issues, the NASA Jet Propulsion Laboratory (JPL) is developing a Mars Helicopter (MH) in collaboration with AeroVironment Inc., NASA Ames Research Center, and NASA Langley Research Center, to create a low altitude Unmanned Aerial Vehicle (UAV) to scout in the vicinity of the rover and explore the red planet [1].

Considering how drastically gravity and atmospheric conditions differ between Earth and Mars, many obstacles must be overcome when designing a flight vehicle for Martian exploration. Because the gravity on Mars is roughly one-third of Earth's, a flight vehicle weighs less on Mars than on Earth; consequently, a flight vehicle would need less thrust to become airborne. However, the reduced thrust required from a lighter vehicle is undermined by the drastic reduction in atmospheric density, which is over 100 times less than that of Earth. In addition, the reduction in temperature, specific heat ratio, and atmospheric gas constant reduce the speed of sound considerably. Further, the low Reynolds number for a rotor operating in a Martian atmosphere has a high impact on rotor performance

Presented at the AHS International Technical Conference on Aeromechanics Design for Transformative Vertical Flight, San Francisco, CA, Jan 16-18, 2018. This is a work of the U.S. Government and is not subject to copyright protection.

due to possible early flow separation on the blade [2].

## Mars Atmospheric Conditions

The atmosphere of Mars is 95% $CO_2$ with the remaining 5% comprised of $N_2$ and other trace gases. The surface temperature is about -80 deg Fahrenheit and, as a consequence of polar $CO_2$ condensation and sublimation, has a seasonal variation of approximately 20% of its planetary atmospheric mass [3]. Table 1 compares the conditions of Mars with Earth [4].

**Table 1. Atmospheric conditions on Earth and Mars.**

| Variable | Earth | Mars |
|---|---|---|
| Density (slug/ft$^3$) | 23.77 x 10$^{-4}$ | 3.88 x 10$^{-5}$ |
| Gravity (ft/s$^2$) | 32.2 | 12.2 |
| Temperature (°F) | 59 | -80 |
| Specific Heat Ratio | 1.40 | 1.29 |

## Experimental Setup

### Planetary Aeolian Laboratory

The Planetary Aeolian Laboratory (PAL) is a 98.5-ft high, 459,090-ft$^3$ volume near-vacuum facility capable of conducting experiments under atmospheric conditions ranging from Earth's atmosphere, approximately 1-bar (1018 mbar), down to 5.5 mbars [5], which is less than the atmospheric pressure of Mars. The facility can be evacuated to its minimum pressure of 5.5 mbars in about 45 minutes, an operation performed by the NASA Ames Thermal Physics Facility's Steam Vacuum System (SVS) [5].

At all atmospheric conditions, the PAL chamber composition is that of Earth's; for non-critical Mach numbers, differences between Earth's (primarily $O_2$ and $N_2$) and Mars' (primarily $CO_2$) atmosphere are thought to be negligible. Due to the high cost to evacuate the PAL, the majority of the PAL testing is done in conjunction with other NASA Ames projects already requiring vacuum; in doing so, the windows of time allotted to PAL vacuum testing are often based on dual-use opportunities. Although not pursued for this project, vacuum testing can be dedicated to the PAL if sufficient funding is in place, allowing for extensive low pressure testing. A picture of the PAL can be seen in Figure 1.

**Figure 1. Planetary Aeolian Laboratory.**

### Martian Surface Wind Tunnel

The Martian Surface Wind Tunnel (MARSWIT), shown in Figure 2, was first put into operation in 1976, and is an open-circuit 43-ft-long atmospheric boundary-layer wind tunnel. The internal cross section is 3.3 (height) by 4 (width)-ft [6]. As the MARSWIT is in the PAL near-vacuum chamber, the wind tunnel can be tested at all atmospheric conditions of which the facility is capable; at 1018 mbar, the wind tunnel can reach wind speeds of 34.5-ft/sec, and at 5 mbars, wind speeds of 328-ft/sec. The tunnel has been used to investigate the physics of particle entrainment under Martian conditions, to test spacecraft instruments under Martian conditions [6], and recently to test rotor performance. All test data presented in this paper were acquired with the wind tunnel drive system turned off.

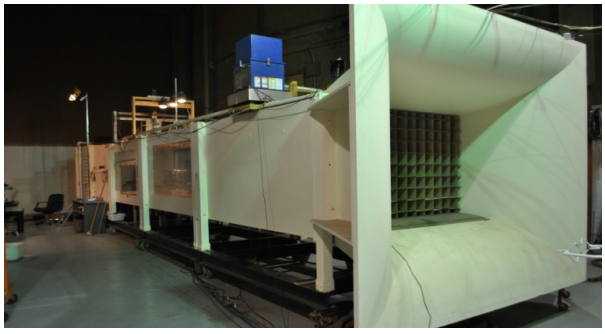

**Figure 2. PAL Martian Surface Wind Tunnel**

### Test Overview

Test hardware was installed into the MARSWIT test section, approximately located midway along

the 43-ft-long wind tunnel. Testing consisted of both single rotor and dual rotor configurations. The single rotor was to test a rotor in nominal helicopter mode. The dual rotor was to resemble the MH's coaxial design, as well as to provide increased rotor thrust representative of the MH design. However, unlike the MH's coaxial system, both rotors in the dual configuration are fixed, rotating in the same direction, at 90 deg orientation. Both the single and dual rotor configurations are shown in Figure 3.

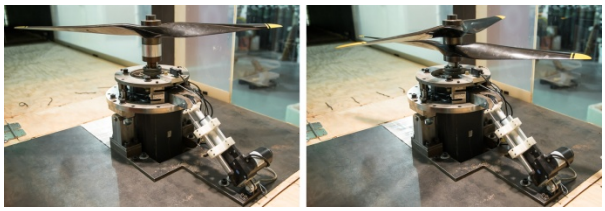

**Figure 3. Left and right images show single and dual rotor configurations tested in the MARSWIT test section, respectively.**

Test hardware was designed such that the rotor could be tested between ±14 degrees angle of attack. For the presented data, all tests were conducted at -14 deg, pitching the test apparatus towards the tunnel inlet. Figure 4 shows the single rotor configuration at 0 deg and -14 deg (forward flight). Figure 5 shows the rotor again at -14 deg, but from downstream of the test section.

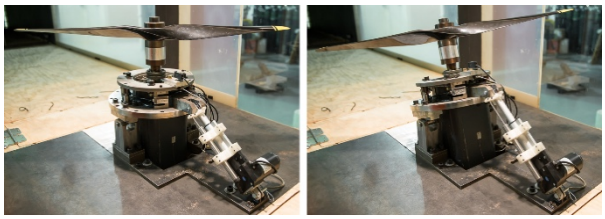

**Figure 4. Left shows single rotor at shaft angle of 0 deg, right shows single rotor at shaft angle of -14 deg.**

**Figure 5. Single rotor at shaft angle -14 deg, looking downstream of the test section.**

Testing was conducted from a pressure range of 1-atmosphere (Earth's atmosphere) down to 8 mbar (conditions which approximate the atmospheric conditions found on Mars).

### Test Model Hardware and Sensors

The primary goals were to collect rotor thrust, RPM, power, torque, motor temperature, and wind speed, as well as chamber pressure, humidity, and temperature, while in forward flight. That said, the following sections discuss the hardware and sensors used to obtain this data, and reference Figure 6 and Figure 7 for location within the MARSWIT.

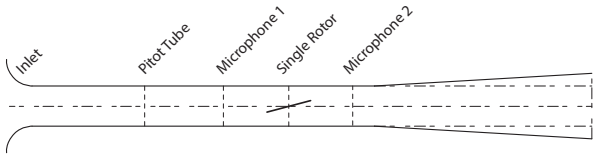


**Figure 6. Side profile of the 43-ft-long MARSWIT.**

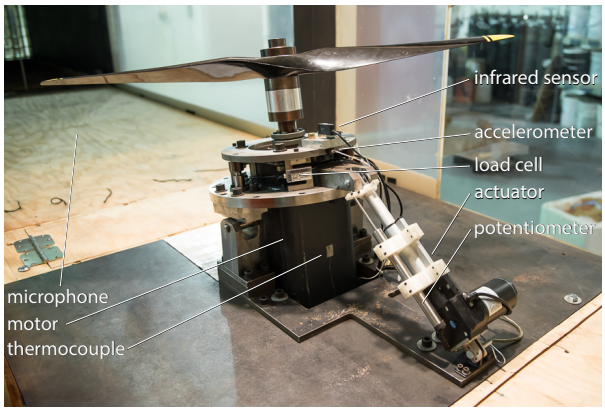


**Figure 7. Hardware and sensor installation within the MARSWIT test section.**

Prior to MH testing in JPL's 25-Foot Space Simulator, a 1-atmosphere rotor hover safety checkout needed to be conducted within the chamber. As part of this effort, the 40x22 rotor was selected in 2015, and tested for this activity [7]. The same rotor blades and motor were used for reduced pressure forward flight testing at NASA Ames Research Center in 2017.

To provide a better understanding of what the MH might experience during forward flight on Mars, the selected rotor was chosen based on the MH's physical dimensions and operating conditions. The projected MH will be equipped with a coaxial rotor system, with rotor disks approximately 3.94-ft in diameter. However, due to restrictions in

MARSWIT test section dimensions, the largest testable rotor was limited to 3.33-ft in diameter, approximately 0.65-ft smaller than what will be installed on the MH. In addition to rotor diameter, the selected rotor was chosen to be operational up to 3000 RPM to match the RPM and hover tip Mach Number of the proposed MH.

The selected rotor is highly twisted and defined by the manufacturer as 40x22. The first number represents the rotor diameter in inches. The second number refers to the forward distance traversed, in inches, for every rotor revolution when acting as a propeller [8].

The motor used for rotor operation is the Siemens Electric AC Motor, model #1FT5104-0AF71-I. This motor was selected for the first ever Martian atmosphere rotor hover testing in 2002, which also took place in the PAL near-vacuum chamber [3]. Because this motor was proven to operate extensively under vacuum, it was chosen again for this test. Measurements included RPM based on a motor encoder and torque based on motor current; both RPM and torque were recorded by the Data Accusation System (DAS). A thermocouple was mounted to the motor for motor temperature monitoring.

An Omron #E3S-AR11 infrared sensor (IR) was used during testing. This is a built-in amplifier photoelectric feedback sensor, which was used to indicate motor RPM. Reflective tape, adhered to the motor shaft, reflects the IR signal once per motor revolution. This sensor was only used to monitor RPM while testing and was not recorded.

To measure rotor thrust, the motor is fixed to three Sensortronics S-Beam load cells, model #60001. Each load cell is single axis and can measure up to 50-lbs within a safe margin. The collective 150-lb measurable weight is required to accommodate the dead weight of the motor and rotor hardware. The load cells were mounted 120 deg apart about the rotor's axis of rotation.

At 1-atmosphere, rotor thrust is much larger than that at reduced pressure. As the PAL is evacuated to Martian pressures, the atmospheric density within the chamber is approximately 100 times less than when at 1-atmosphere. Consequently, the load cells are operating at their minimum specifications when measuring thrust at extremely low chamber pressures. This will be discussed in the Testing Challenges section of the paper.

MARSWIT wind speed is determined from a 1 mbar differential pressure transducer attached to a pitot-static probe, located forward of the test section. The transducer, a model Barocell-590, was on a heated plate located in the PAL control room to minimize temperature drift. Wind speed is measured only in the direction of air entering the MARSWIT inlet.

To determine the test hardware structural resonance, a resonant frequency test was performed for each rotor configuration. Frequencies with the highest amplitude occur around 1900 RPM for the single and dual rotor configurations.

Vibrations were monitored throughout testing by two uniaxial 5g Kistler accelerometers mounted 90 degrees apart, on a plane perpendicular to the axis of rotation. Accelerometer installation was for the sole purpose of monitoring amplitude throughout testing, particularly around determined resonant frequencies.

Acoustics measurements (not presented in this paper) were taken by two microphones, placed 60 inches ahead and behind the test section, equidistant from the axis of rotation. The microphones and amplifiers are part of a G.R.A.S. Sound & Vibration System.

Absolute chamber pressure, density, humidity, and temperature sensors located in the PAL vacuum chamber were used for this test. The Setra 204 absolute pressure transducer and a Wallace and Tiernan FA129 absolute pressure gauge were used to measure chamber pressure. Lastly, humidity and temperature were measured by a Vaisala DMP248.

**Data Acquisition Systems**

All sensor cables bridge the vacuum chamber wall to the PAL control room, where they are recorded to one of two data systems, an AstroMed Dash 18X (AstroMed) and a PAL LabVIEW system. The AstroMed is a 14-bit DAS used for real-time monitoring and data recording, with real-time sensor calibration and filter application. Rotor thrust, RPM, power, torque, acoustics, wind speed, and stand vibration were recorded to this system.

The PAL LabVIEW system recorded absolute chamber pressure, density, humidity, and temperature.

Post-processed data records are merged based on the time stamp of each DAS. Once merged, the data undergoes zero-point subtraction of load cell weight, torque, and acoustic tares. Periodic zero-point subtraction became particularly important when measuring rotor thrust, as the three load cells demonstrated drift during extended operation; routine zero-points helped capture and mitigate this behavior.

## Test Matrix

Both single and dual rotor configurations were tested over a pressure range of 1018 to 8 mbars, wind speeds up to 49 ft/sec, and rotor speeds up to 3000 RPM at a fixed forward flight shaft angle of -14 deg. For the data presented, the MARSWIT drive system was turned off; measured velocity was from rotor operation or PAL facility wind recirculation itself. All data presented and discussed herein are from Reference 9.

Figures 8 and 9 show PAL chamber pressure against the time between data points collected for single and dual rotor configurations over the course of a single chamber pressure cycle. Collected data can be broken into four facility operational categories: pressure decrease (pump down), constant pressure, pressure drift, and pressure increase (pump up).

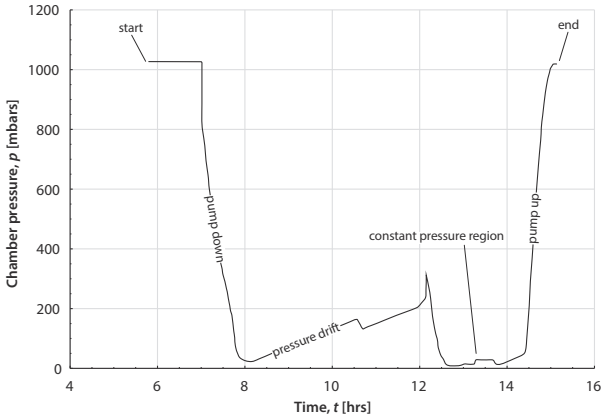


**Figure 8. PAL absolute chamber pressure plotted against the time single rotor data was collected.**

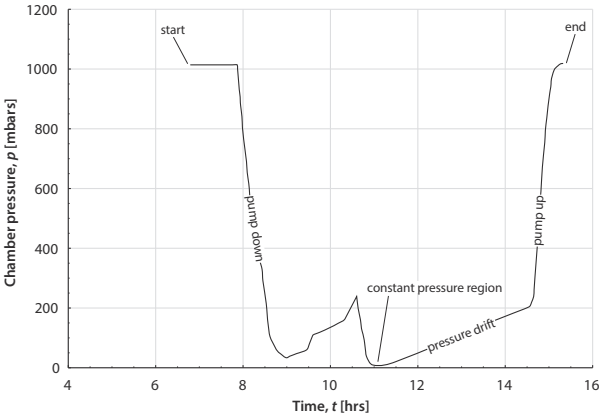


**Figure 9. PAL absolute chamber pressure plotted against the time dual rotor data was collected.**

### Pressure Decrease

The PAL can evacuate from 1018 to 5 mbar in approximately 45-minutes. To measure rotor thrust as a function of decreasing pressure, rotor RPM was held constant for both single and dual rotor configurations while pressure decreased. The RPM chosen for each configuration depended on test stand resonant frequencies and rotor vibration at 1-atmosphere. These were 2100 and 1250 RPM for the single and dual rotor configurations, respectively.

### Constant Pressure

After the PAL chamber had been evacuated to less than 50-mbars, the single rotor was held constant at approximately 28, 14, and 8 mbar; at each of these pressures, the single rotor was tested at 0, 2100, 2500, 2800, and 3000 RPM. While reduced pressure was held constant, the dual rotor was only tested at 8 mbar, and at 3000 RPM.

### Pressure Drift

When the PAL vacuum is shut off, pressure within the PAL can be sustained, but experiences a drift at a rate of approximately 1 mbar per minute. To provide ample amount of data points while simultaneously minimizing the amount of pressure drift, 15-second data points were collected; this corresponded to approximately 0.25 mbar drift for each data point collected.

While PAL pressure drifted, data was collected successively for both single and dual rotors over a

pressure range of 30 to 200 mbar at 0, 2100, 2500, 2800, and 3000 RPM.

### Pressure Increase

As pressure is increased, single and dual rotors are set back to 2100 and 1250 RPM, respectively, the same RPMs used during chamber pump-down. While pressure increased, data was collected at pressures from approximately 200 to 1018 mbar.

## Experimental Results

### Rotor Performance at 1-Atmosphere

Single and dual rotors, although limited in RPM at 1-atmosphere, generated relatively high thrust in the MARSWIT test section. The table below lists the RPM and corresponding single and dual rotor thrust measured at 1-atmosphere.

**Table 2. RPMs tested at 1-atmosphere, with corresponding single and dual rotor thrust (lb) and power (W).**

| | Single Rotor | | Dual Rotor | |
|---|---|---|---|---|
| RPM | Thrust | Power | Thrust | Power |
| 0 | 0 | 0 | 0 | 0 |
| 600 | 3.0 | 52.3 | 5.1 | 75.0 |
| 700 | 4.3 | 88.0 | 7.0 | 140.2 |
| 800 | 5.6 | 134.0 | 9.0 | 230.2 |
| 900 | 7.0 | 195.8 | 11.5 | 343.5 |
| 1000 | 8.5 | 266.9 | 14.3 | 485.9 |
| 1100 | 10.3 | 355.4 | 17.4 | 666.4 |
| 1200 | 11.9 | 458.4 | 20.7 | 879.9 |
| 1300 | 14.1 | 575.5 | 24.1 | 1131.6 |
| 1400 | 16.3 | 720.6 | 28.3 | 1429.1 |
| 1500 | 18.3 | 880.0 | | |
| 1600 | 21.2 | 1078.4 | | |
| 1700 | 23.5 | 1292.2 | | |
| 1800 | 26.7 | 1540.4 | | |
| 2000 | 33.2 | 2120.3 | | |
| 2100 | 36.4 | 2457.0 | | |

For these results, for single rotor operation in the MARSWIT, tunnel airspeeds from 3.8 ft/sec to 15.2 ft/sec were measured; tunnel airspeeds from 5.5 ft/sec to 11.65 ft/sec were measured for the dual rotor within reduced RPM range.

Based on the proportional change in air density with reduced pressure, rotor thrust should be roughly proportional to pressure for a fixed RPM (in hover). This reduction in thrust allowed the rotor RPM to be safely increased up to the motor maximum of 3000 RPM at lower chamber pressures without exceeding load cell steady or dynamic load limits.

### Rotor Performance as Pressure Decreased

As air is pumped into or out of the PAL vacuum chamber, experimental rotor thrust was observed to be near-linear with absolute chamber pressure. Figures 10 and 11 show rotor thrust and power data for the single rotor operating at 2100 RPM and dual rotor at 1250 RPM while chamber pressure is reduced. However, data collected while air was evacuated was likely influenced by wind recirculation within the PAL chamber. These effects are discussed in the Testing Challenges section of the paper.

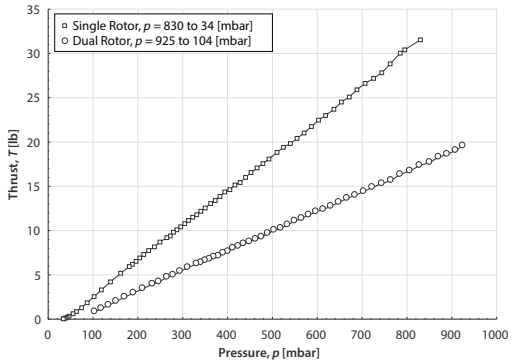


**Figure 10. Rotor thrust measured as chamber pressure was monotonically decreased. Single rotor was held constant at 2100 RPM and dual rotor at 1250 RPM.**

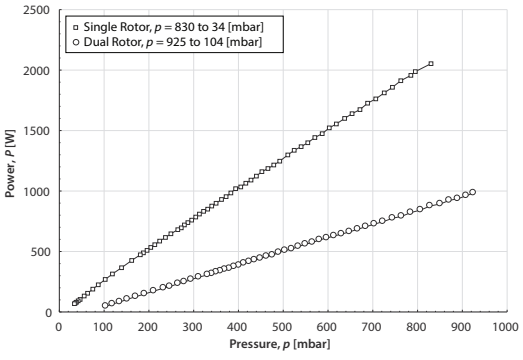


**Figure 11. Rotor power as chamber pressure was monotonically decreased. Single rotor was held constant at 2100 RPM and dual rotor at 1250 RPM.**

### Rotor Performance at Constant Pressure

Constant chamber pressures of 8, 14, and 28 mbar were selected for testing, based on atmospheric densities found near the Martian surface.

The following three plots show single rotor thrust as a function of $RPM^2$ at 8, 14, and 28 mbar. Thrust is expected to be linear with $RPM^2$ for a purely hovering rotor, which is clearly shown to be true for measurements at 14 and 28 mbar, but not for measurements at 8 mbar. From the testing at 14 and 28 mbar, the low and almost constant advance ratio for all test conditions (see below) allows for the apparent linear thrust variation with $RPM^2$ at these low pressures.

As discussed in Reference 9, the difficulties of measuring wind speed inside the wind tunnel, even incremental changes in wind speed, were problematic during the 8 mbar running. Facility generated circulation flow inside the tunnel (other than rotor induced flow) during data acquisition was present, uncontrolled, and unmeasured, invalidating the wind speed sensor. It is also believed that the load cells sensitivity and accuracy for thrust measurements contribute to this 8-mbar data scatter, although a general trend in the thrust data is observed.

For 14 mbar data (Figure 13), measured tunnel airspeeds yielded advance ratios of 0.080 at 2086 RPM (29.0 ft/sec wind speed) to 0.093 at 2975 RPM (48.5 ft/sec). These airspeeds are within the design range for the Mars Helicopter forward flight speed [2]. For the 28 mbar data (Figure 14), the corresponding values are advance ratios of 0.054 at 2087 RPM (19.6 ft/sec) to 0.060 at 2976 RPM (30.9 ft/sec). These measured airspeeds indicate a noticeable facility air re-circulation in the MARSWIT tunnel itself at these test conditions.

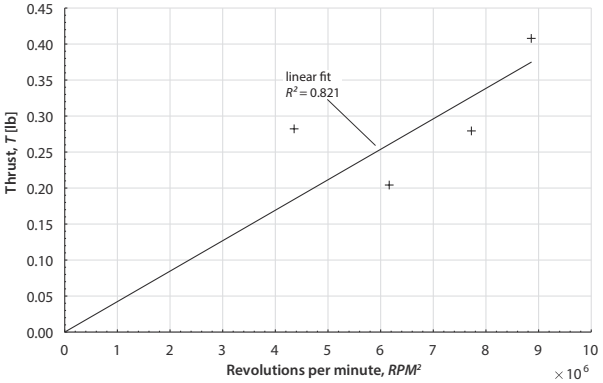


**Figure 12. Plot of Thrust vs $RPM^2$ for the single rotor at 8 mbar.**

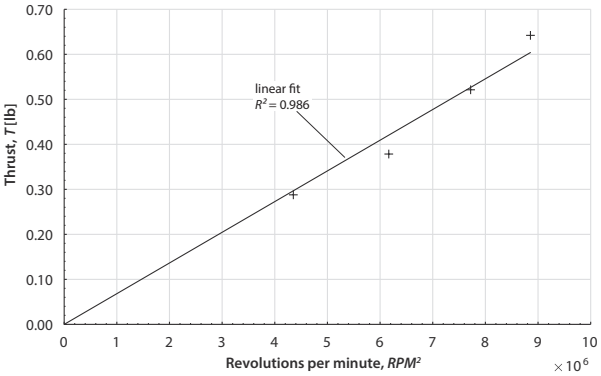


**Figure 13. Plot of Thrust vs $RPM^2$ for the single rotor at 14 mbar.**

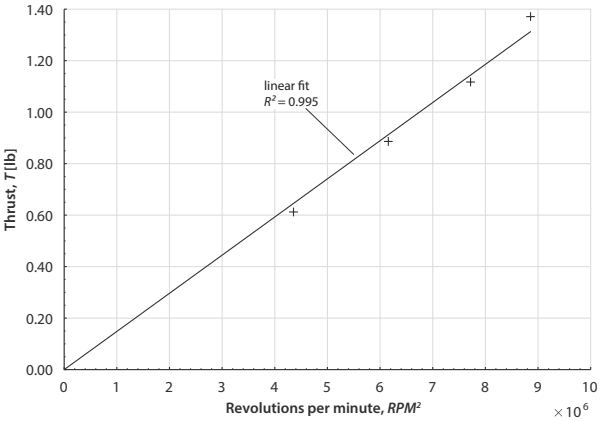


**Figure 14. Plot of Thrust vs $RPM^2$ for the single rotor at 28 mbar.**

### Rotor Thrust Sweeps from 30-200 mbar

Once the PAL is disconnected from SVS, the PAL absolute pressure increases at approximately 1 mbar per minute. While this occurred, single and dual rotor configurations were swept through RPMs of 0, 2100, 2500, 2800, and 3000 successively as pressure increased from 30 to 200 mbar. The single rotor RPM was swept 14 times, and the dual rotor 15 times. Curve fits of thrust vs $RPM^2$ for both single and dual rotor configurations can be seen in Figures 15 and 16. The data is tabulated in Reference 9.

The roughly linear relationship between thrust and $RPM^2$ is similar to the 14 mbar and the 28 mbar results (Figures 13 and 14, respectively) and is further discussed in the next section.

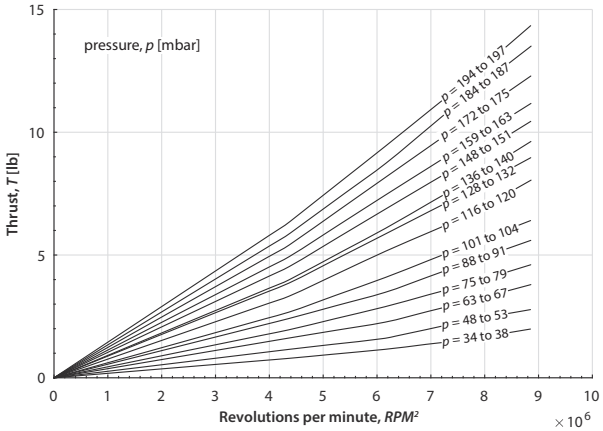


**Figure 15. Single rotor Thrust vs RPM$^2$ as chamber pressure was increased from about 30 to 200 mbar.**

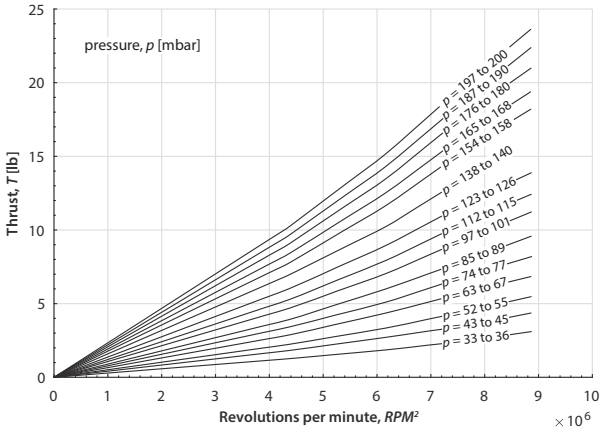


**Figure 16. Dual rotor Thrust vs RPM$^2$ as chamber pressure was increased from about 30 to 200 mbar.**

Rotor Wind Velocity from 70-200 mbars

All tests were conducted with the wind tunnel drive system turned off. Given this, when chamber pressure was held constant or with minimal drift, wind generation within the MARSWIT was due to rotor operation once the effects of facility air evacuation pumping had decayed.

Figure 17 and Figure 18 show single and dual rotor wind velocity in MARSWIT as chamber pressure increased from about 70 to 200 mbar at a rate of 1 mbar per minute, as well as extrapolated 1-atmosphere testing in the MARSWIT. For each pressure range shown, the single rotor was swept through the following RPMs: 0, 2100, 2500, 2800, and 3000. During these sweeps, the measured wind tunnel airspeed for the single rotor corresponded to very low advance ratios of 0.033 (75 mbar) to 0.041 (187 mbar). And for the dual rotor sweeps, advance ratios of 0.040 (74 mbar) to 0.051 (200 mbar) were measured. These small values are comparable to other hovering rotor operating conditions in atmospheric wind tunnels (small scale or full scale).

It is interesting to note that the velocities measured during the pressure sweeps for the single rotor (Figure 17) are less than the values measured during the constant 14 mbar and 28 mbar testing discussed above (up to 48.5 ft/sec for 14 mbar testing and 30.9 ft/sec for the 28 mbar testing). This is further evidence that the facility-generated air circulation was present during these very low constant-pressure, single rotor RPM sweeps. Additionally, the testing at 28 mbar took place immediately following testing at 14 mbar indicating the likelihood of facility flow circulation reducing during this portion of the testing.

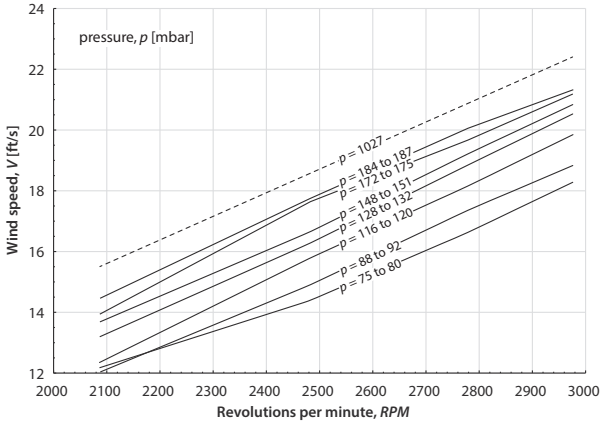


**Figure 17. Single rotor MARSWIT wind velocity as pressure increased from 75 to 187 mbar, as well as extrapolated 1-atmosphere.**

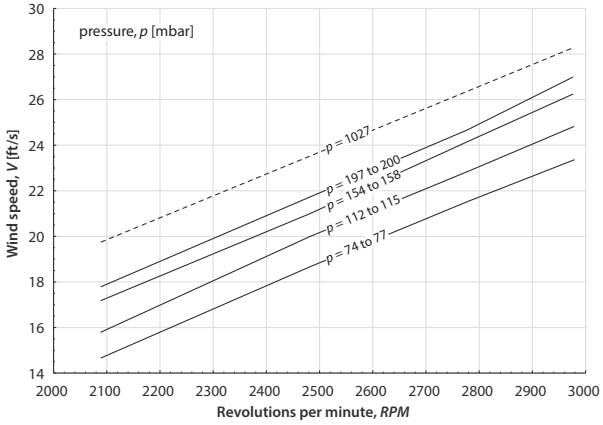


**Figure 18. Dual rotor MARSWIT wind velocity as pressure increased from 74 to 200 mbar, as well as extrapolated 1-atmosphere.**

Wind speed, shown previously in Figures 17 and 18, was measured using a pitot-static probe located

forward of the test section. The equation for induced flow through the rotor can help describe why the wind speed remains fairly constant for the different pressures tested.

$$v_{induced} = \sqrt{\frac{T}{2\rho A}} \quad (1)$$

As rotor thrust was experimentally shown to be nearly linear with absolute chamber density (Figure 10), this implies that $T/\rho$ should remain near-constant when testing at different atmospheric pressures at constant RPM. That being the case, as chamber pressure decreases, rotor induced velocity and therefore measured wind velocity decreases by a predictable amount. One reason for this is the lower lift coefficients at very low Reynolds numbers. The reduced lift at subcritical Reynolds numbers will directly lower the thrust values and thereby reduce velocity to some extent [2].

Measured Rotor Power and Torque

Measured torque and power are based on the current supplied to the motor as rotor RPM changes. Experimental data shows that as chamber pressure is decreased, the motor torque required for a given thrust value increased. Figure 19 and Figure 20 demonstrate this behavior for the single rotor swept from 0 to 3000 RPM at 8, 14, 28, 128, 194, and 1018 mbar; for pressures of 128 and 194 mbar, the chamber drifted at 1 mbar per minute. The linear curve fits in these figures (and future figures) are shown to elucidate the experimental data trends and are not physics based.

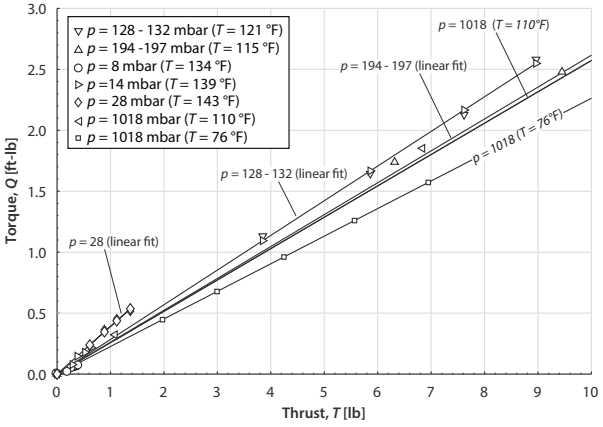


**Figure 19. Torque vs thrust curves for the single rotor operating at 8, 14, 28, 128, 194, and 1018 mbar.**

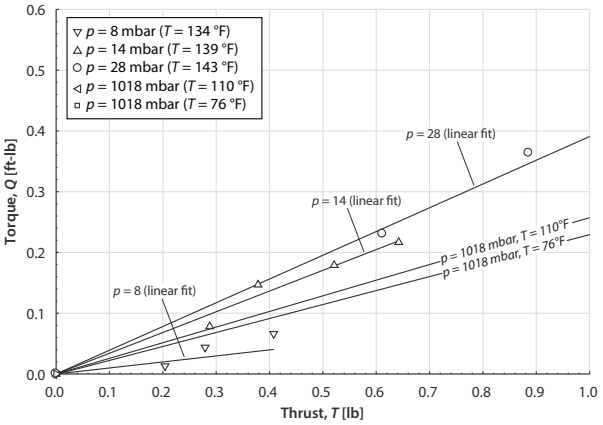


**Figure 20. Close up of Figure 19, only showing torque vs thrust curves at 8, 14, and 28 mbar.**

It seems possible that as pressure is reduced, the rotor becomes increasingly inefficient, consuming higher amounts of torque and power with minimal output thrust. However, there are a few variables which might contribute to this behavior.

To measure rotor thrust, the motor and rotor assembly is suspended from a metal plate, which mounts directly to the three single axis load cells. Before data was collected, it was observed that the initial heating of the motor helped stabilize the thermal effects on load cells. Because motor cooling depends primarily on heat conduction from the test stand hardware through convection with air, as chamber pressure and density decreases, the air's convective capability also decreases. This makes convection cooling less effective, particularly at extremely low pressures. At reduced pressures and 3000 RPM, motor temperatures increased to as high as 150 deg F.

In Figure 21, several 1-atmosphere, dual-rotor thrust-vs-RPM$^2$ sweeps are plotted as motor temperature increases for low thrust values. From this plot it would appear that motor temperature effects would be less than 0.25 lb at the lowest pressures tested, but within the range of data scatter in Figure 12 at 8 mbar for single rotor testing. However, for the same data points shown in Figure 21, Figures 22 and 23 show that measured torque and power were not significantly affected by variations in motor temperature.

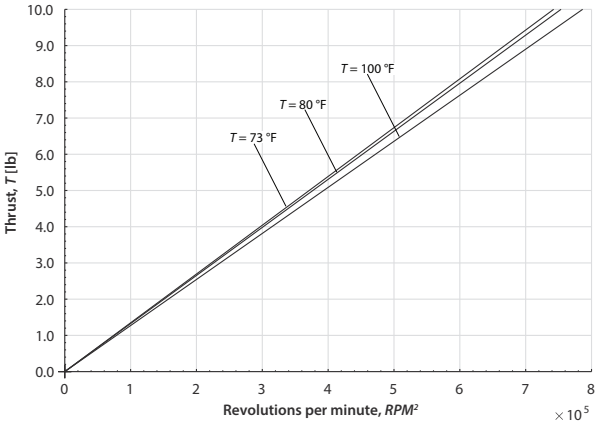


**Figure 21. Dual rotor Thrust vs RPM$^2$ at 1-atmosphere as motor temperature increased.**

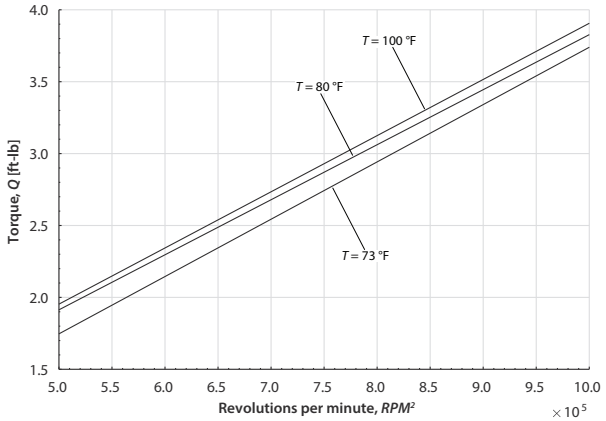


**Figure 22. Dual rotor Torque vs RPM$^2$ at 1-atmosphere as motor temperature increased. Vertical and horizontal axes shortened to show deviation between points.**

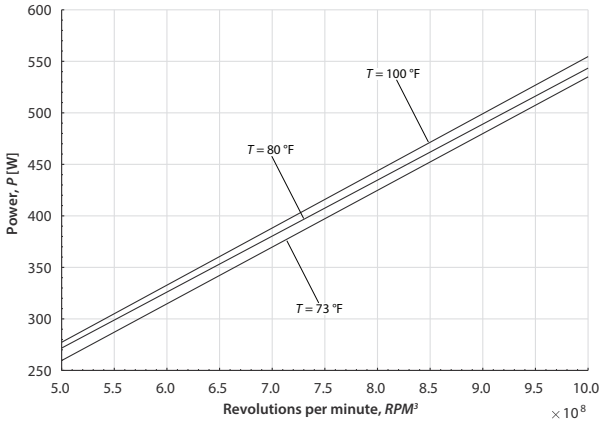


**Figure 23. Dual rotor Power vs RPM$^3$ at 1-atmosphere as motor temperature increased. Vertical and horizontal axes shortened to show deviation between points.**

Air circulation within the PAL chamber also impacted measured wind speed and rotor thrust. Once pressure is held constant or drifting at 1 mbar per minute, facility air circulation settles, producing torque vs thrust curves (Figures 19) much closer to that at 1-atmosphere.

## Experiment vs Simulation

### CFD Introduction

Although there has been recent interest in UAVs operating in low pressure environments, this still is a relatively new area of research. Consequently, experimentation plays a vital role in validating CFD, and vice versa. The experimental results for the single rotor in free field hover and MARSWIT forward flight testing will now be compared against computer simulation at 1–atmosphere (1018 mbar), as well as at 28 mbar.

#### 40x22 AWT Airfoil Tables

To generate the CFD airfoil tables for the AWT rotor, the propeller blade was measured using the CreaformMetraScan-70, a 3D optical laser scanner. The resulting point cloud is processed by fitting profile curves and surfaces to reconstruct the 3D CAD model of the AWT rotor. The airfoils are used to extract the magnitude and location of maximum thickness and camber to evaluate the critical radial station selection. Radial stations at r/R = 0.29, 0.58, and 0.78 were chosen as the critical airfoils.

#### Approach

The code, C81Gen, is used to generate aerodynamic coefficients for span-wise locations along the rotor. C81Gen is developed to create C81 format tables for a user-specified range of Angle-of-Attack/Mach pairs. C81Gen runs the two-dimensional, time-dependent compressible Reynolds Averaged Navier Stokes (RANS) solver ARC2D with structured body fitted viscous gridding. The program uses an implicit finite-difference method to solve two-dimensional thin-layer Navier Stokes equations [2]. Turbulence modeling in C81Gen utilizes the Spalart-Allmaras (SA) turbulence model. For this study, C-grids where used and all airfoils having normalized chord lengths of $c = 1.0$ with the far field located at $50c$. For the C-grid, the number of points in stream-wise, normal, and wake direction are specified. The $y^+$ value was kept around $y^+ = 1.0$ for all cases investigated. Airfoil tables at 1-atmosphere and 7 mbar were generated and used in this study.

The code Rotorcraft CFD (RotCFD) is used to predict the rotor performance for free field and wall bounded tunnel conditions. RotCFD is a mid-fidelity CFD tool specifically designed for rotorcraft design efforts [10]. Rotorcraft Unstructured Solver (RotUNS) is a module within RotCFD that solves the three-dimensional incompressible unsteady RANS equations (URANS) on a Cartesian unstructured grid using an implicit finite-volume method. The Semi-Implicit Method for Pressure-Linked Equations Revised (SIMPLER) is used to link the equations. Turbulence is modeled in RotCFD using the k-ε turbulence model with special wall function. A rotor is modeled using a Blade-Element Model (BEM) and interacts with the flow-field through the momentum it imparts on the flow. RotCFD has been successfully used for various analyses on complex rotor flows [11] [12] at a fraction of the computational budget when compared to a complete Navier Stokes solution for a rotating body-fitted rotor. A detailed description of the AWT rotor model can be found in Reference 8.

## Result Comparisons

1018-mbar Rotor in Hover

Both single and dual rotors were tested at 1-atmosphere in hover [7], which were tested approximately 10-ft off the ground, thrusting upward. No torque measurement capability was in place for this testing. The hovering rotor computational grid used in RotCFD can be seen in Figure 24.

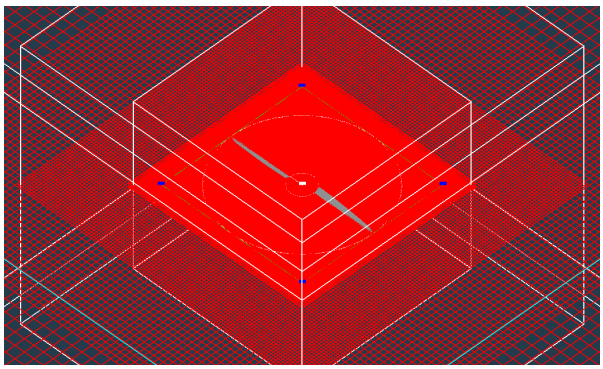

**Figure 24. RotCFD grid for the 40x22 AWT single rotor in hover.**

Single rotor experimental thrust results compared with RotCFD simulation can be seen in Figures 25 (single rotor) and 26 (dual rotor). Simulated thrust results correlated well with free field, 1-atmosphere experimental testing.

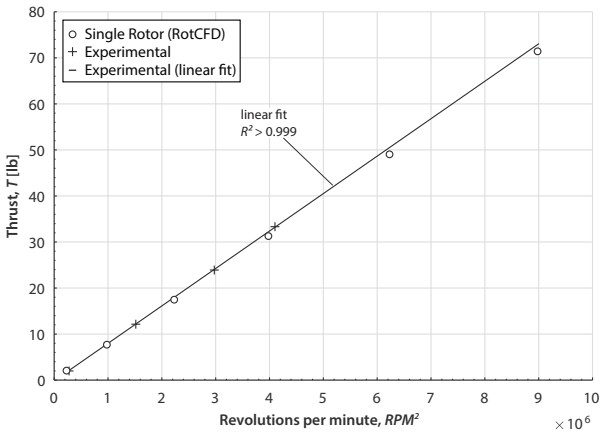


**Figure 25. Experiment vs RotCFD: 1-atmosphere Thrust vs RPM$^2$ for single rotor tested in hover.**

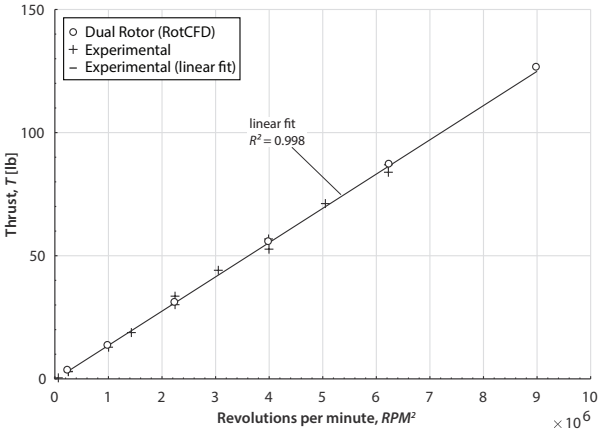


**Figure 26. Experiment vs RotCFD: 1-atmosphere Thrust vs RPM$^2$ for dual rotor tested in hover.**

1018-mbar Rotor Forward Flight

Experimental 1-atmosphere MARSWIT data (Table 2) was also compared with the simulation for the single rotor testing. To match experimental work, the single rotor at -14 deg and tunnel were modeled in RotCFD. Figure 27 shows a RotCFD grid of the MARSWIT test section and single rotor in forward flight.

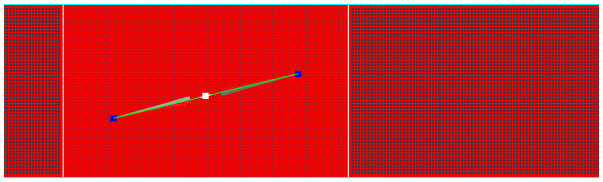

**Figure 27. Zoomed in image of RotCFD grid overlaying the MARSWIT test section. Tunnel wind direction is left to right.**

The tunnel grid is a constant area duct with the cross-sectional dimensions of the MARSWIT test section. The inlet boundary condition for a given RPM was given by the following equation in ft/sec.

$$V_{BC\ Tunnel} = 0.0075 * RPM \quad (2)$$

First, comparing measured rotor thrust generation between free field (Figure 25) and the MARSWIT tunnel installation (Figure 29), rotor thrust as a function of $RPM^2$ is virtually identical. Unfortunately, because torque was not measured in the free field testing, no definitive observation can be made for MARSWIT facility effects on rotor performance during 1-atmosphere testing. Figure 28 shows a flow visualization of simulated MARSWIT 1-atmosphere results.

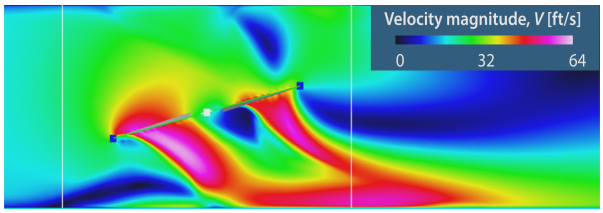


**Figure 28. 1-atmosphere RotCFD flow visualization for single rotor operating at 2000 RPM.**

From the correlation with RotCFD, simulation values for thrust show a 6 percent decrease from experiment (Figure 29) and torque (Figure 30) is under predicted by about 30 percent for the single rotor test configuration. Since both thrust and torque are under predicted, the predicted power as a function of thrust is better matched with experiment (Figure 31), particularly at low thrust levels where facility installation effects might have less of an effect on measured rotor performance.

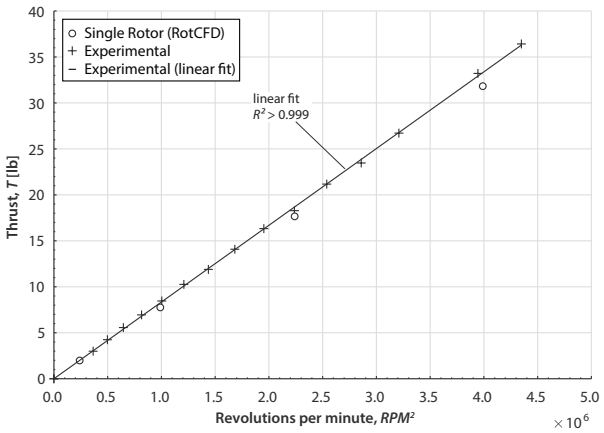


**Figure 29. Experiment vs RotCFD: 1-atmosphere Thrust vs $RPM^2$ for single rotor in MARSWIT.**

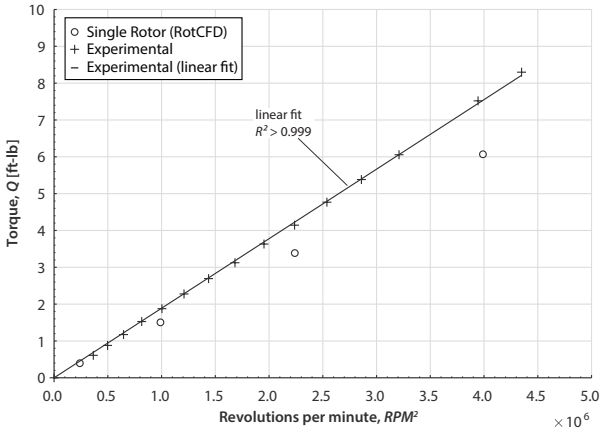


**Figure 30. Experiment vs RotCFD: 1-atmosphere Torque vs $RPM^2$ for single rotor in MARSWIT.**

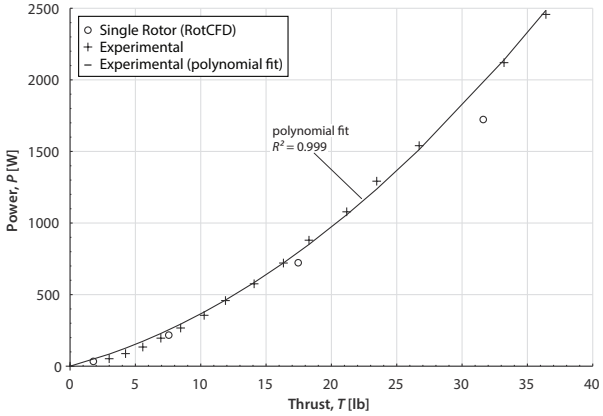


**Figure 31. Experiment vs RotCFD: 1-atmosphere Power vs Thrust for single rotor in MARSWIT.**

## 28-mbar Rotor Forward Flight

The analyzed 28.7 mbar data was taken with the PAL chamber pressure being held constant and after the air circulation had quieted, so the wind speeds used for the RotCFD inflow boundary conditions were the measured MARSWIT tunnel speeds (Table 3).

**Table 3. 28 mbar test conditions analyzed.**

| RPM | Wind Speed (ft/s) | Advanced Ratio |
|---|---|---|
| 2100 | 19.6 | 0.054 |
| 2500 | 25.4 | 0.059 |
| 2800 | 28.2 | 0.058 |
| 3000 | 30.9 | 0.060 |

Figure 32 shows a flow visualization of simulated rotor 28 mbar results at 3000 RPM. Plots for experimental single rotor performance are compared with simulation in Figures 33 through 35. RotCFD under predicts measured rotor thrust and torque. Thrust is under predicted by about 35 percent

(Figure 33) and rotor torque (Figure 34) is under predicted by about 20 percent at 3000 RPM. The under predictions for thrust are substantially larger than the 1-atmosphere rotor thrust under predictions on a percentage basis. Both torque under predictions are comparable on a percentage basis. The greater discrepancy in thrust prediction at reduced pressure may be due to the airfoil lift tables or different facility effects at reduced pressure (wall boundary layer size, turbulence levels), or perhaps even inflow discrepancies in the predictions since the MARSWIT test section flow quality has never been characterized for this test configuration but was modeled as uniform.

When comparing power as a function of thrust (Figure 35), the predicted power is over predicted at a given thrust. The increasing under prediction of thrust with increasing RPM makes the predictions overly conservative (too high) in power prediction.

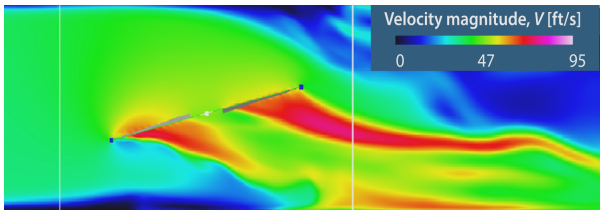


**Figure 32. 28 mbar RotCFD flow visualization for single rotor operating at 3000 RPM.**

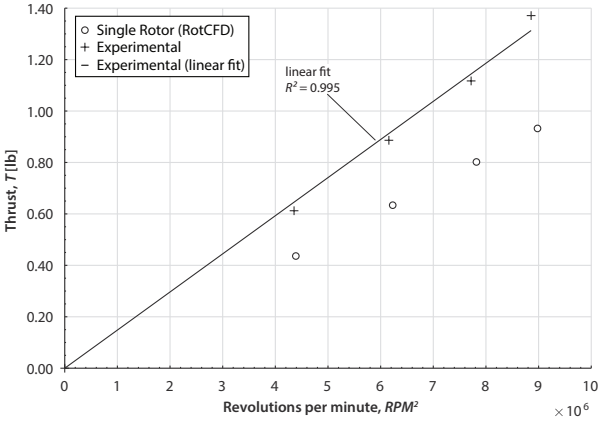


**Figure 33. Experiment vs RotCFD: 28 mbar Thrust vs RPM$^2$ for single rotor in MARSWIT.**

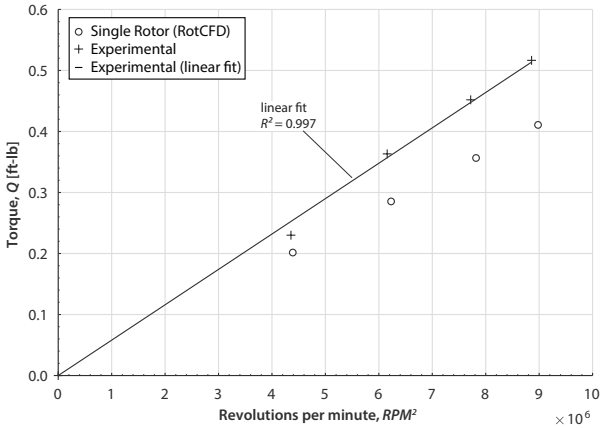


**Figure 34. Experiment vs RotCFD: 28 mbar Torque vs RPM$^2$ for single rotor in MARSWIT.**

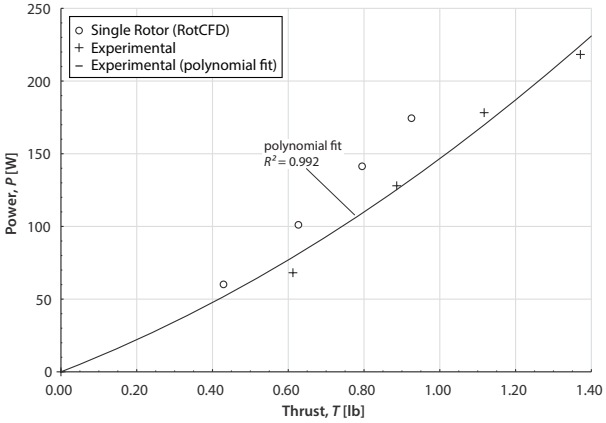


**Figure 35. Experiment vs RotCFD: 28 mbar Thrust vs Power for single rotor in MARSWIT.**

## Testing Challenges

Rotor performance measurements were determined to be affected by chamber recirculation within the PAL, motor thermal effects, load cell hysteresis, and load cell sensitivity and range. Subsequent sections discuss the extent to which each affected load cell measurements.

### PAL Chamber Recirculation

The physical location in which air is pumped out of or into the PAL chamber is relatively close in proximity to the MARSWIT inlet. Given this, measured tunnel wind speed is affected as chamber pressure is rapidly increased or decreased, showing increased or decreased wind speed, depending on test condition. As such, experimental data is presented herein only for data points collected while PAL pressure was held constant or drifting at

1 mbar per minute, which was shown to have minimal effect.

### Motor Thermal Effects

Motor temperature affects load cell measurements. Higher motor temperatures correspond to slightly reduced thrust measurements (Figure 21). To curb this behavior, the motor was heated at the beginning of each test to help reduce thermal effects. That said, rapid changes in chamber pressure had a more significant impact on load cell measurements than motor thermal effects.

### Load Cell Hysteresis

Hysteresis was observed in the three single-axis load cells. This behavior is more often seen when analyzing data for decreasing rotor RPM at near constant pressure. This may be in part to the unloading of the load cell system as thrust is reduced. Due to very low thrust levels, this hysteresis is most noticeable at reduced pressures.

### Load Cell Sensitivity and Range

The three 50-lb single axis load cells were chosen to accommodate the dead weight of the motor and rotor assembly. At 1-atmosphere, the single rotor is capable of producing about 70-lbs thrust, and the dual rotor about 128-lbs thrust (3000 rpm, isolated rotor hover operation). As pressure is reduced, rotor thrust can drop to a fraction of a pound, particularly when pressure is below 14 mbar. Because of this, measured rotor thrust at extremely low atmospheric density and pressures can vary, particularly due to the issues mentioned above.

### Low Pressure Data Collection

The goal of this experiment was to capture rotor behavior over a pressure range of 1018 mbar down to 8 mbar. When used to collect rotor thrust at 8 mbar, the load cells were operating at minimum sensitivity levels. Although this was appropriate for the purposes of this test, load cells with a smaller range would be best suited for capturing data at extremely low pressures. If such a test were performed, data could only be collected below certain atmospheric conditions as rotor thrust quickly increases as pressure increases.

## Future Work

Previously in this paper, both single and dual rotor thrust was compared with RotCFD simulations. Future work could include collecting 1-atmosphere rotor power and torque, in addition to rotor thrust. Further, both rotor configurations should be tested in the PAL at reduced pressure but outside of the MARSWIT. Both experimental cases, 1-atmosphere and reduced pressure, should then be compared with RotCFD results modeling hover operation, including facility and test stand effects.

## Conclusions

Experimental rotor forward flight testing at 1-atmosphere down to Mars atmospheric pressures was challenging but overall successful for both single and dual rotor configurations. Experimental rotor thrust, torque, and power were collected at constant pressures of 8, 14, and 28 mbar, 30 to 200 mbar while pressure drifted at 1 mbar per minute, and at 1-atmosphere. In addition to rotor behavior, rotor-induced wind tunnel velocity was compared from 70 to 200 mbar against results at 1-atmosphere for both single and dual rotors.

Predicted RotCFD results correlated well with experimental 1-atmosphere free-field hover thrust data for both single and dual rotors. For operation in the MARSWIT at 1-atmosphere, single rotor thrust is well predicted but torque and power are under predicted by about 30 percent. At 28 mbar in the MARSWIT, the single-rotor thrust is under predicted by about 35 percent and torque by about 20 percent. Rotor performance as a function of power versus thrust is relatively well predicted at 1-atmosphere but overly conservative in power prediction for a given thrust at 28 mbar.

## References


[1] "Proceedings of the 10th International Planetary Probe Workshop," vol. 1, p. 8120, 2013.

[2] W. J. F. Koning, W. Johnson, and B. G. Allen, "Generation of Mars Helicopter Rotor Model for Comprehensive Analyses," in Aeromechanics Design for Transformative Vertical Flight, San Francisco, CA, January 2018.

[3] R. Young, L., Aiken, E.A., Derby, M.R., Johnson, J.L., Navarete, J., Klem,, J., Demblewski, R., Andrews, J., Torres, "Engineering Studies into Vertical Lift Planetary Aerial Vehicles," AHS International Meeting on Advanced Rotorcraft Technology and Life Saving Activities, Tochigi, Japan, November 2002.

[4] "U.S. Standard Atmosphere." [Online]. Available: https://www.engineeringtoolbox.com/standard-atmosphere-d_604.html. [Accessed: 31-Dec-2017].

[5] "NASA - Planetary Aeolian Laboratory." [Online]. Available: https://www.nasa.gov/centers/ames/business/planetary_aeolian_facilities.html. [Accessed: 03-Aug-2017].

[6] "PAL | The Ronald Greeley Center for Planetary Studies." [Online]. Available: https://rpif.asu.edu/index.php/pal/. [Accessed: 23-Nov-2017].

[7] M. McCoy, A. J. Wadcock, and L. A. Young, "Documentation of the Recirculation in a Closed-Chamber Rotor Hover Test," NASA TM-2016-219162, August 2016.

[8] W. J. F. Koning, "Generation of Performance Model for the Aeolian Wind Tunnel (AWT) Rotor at Reduced Pressure," NASA CR-2018-219737, January 2018.

[9] G. A. Ament, W. J. F. Koning, and L. Meyn, "Isolated Rotor Forward Flight Testing from One Atmosphere Down to Martian Atmospheric Densities," NASA CR-2018-219736, January 2018.

[10] R. G. Rajagopalan, V. Baskaran, A. Hollingsworth, A. Lestari, D. Garrick, E. Solis, and B. Hagerty, "RotCFD - A Tool for Aerodynamic Interference of Rotors: Validation and Capabilities," American Helicopter Society International - Future Vertical Lift Aircraft Design Conference, San Francisco, CA, January 2012.

[11] L. A. Young, G. K. Yamauchi, and G. Rajagopalan, "Simulated Rotor Wake Interactions Resulting from Civil Tiltrotor Aircraft Operations Near Vertiport Terminals," 51st AIAA Aerospace Sciences Meeting, Grapevine, TX, January 2013.


## Acknowledgements


The authors would like to thank Farid Haddad for his expertise in electronics and controls during experimental setup, Ken Smith for operation of the PAL vacuum facility, Eduardo Solis for scanning the 40x22 AWT-rotor for RotCFD simulation, Larry Meyn for data reduction, Larry Young for originally inspiring the idea of forward flight testing under Martian conditions, and William Warmbrodt for his continued support and guidance on the project. Lastly, a thank you to the 2016-17 Aeromechanics Interns for their support during data collection.